SCIENTIFIC REP⚙RTS

Hybrid α-Fe$_2$O$_3$@Ni(OH)$_2$ nanosheet composite for high-rate-performance supercapacitor electrode

Hong Jiang[1], Haifeng Ma[2], Ying Jin[2,3], Lanfang Wang[2], Feng Gao[1] & Qingyi Lu[2]

In this study, we report a facile fabrication of ultrathin two-dimensional (2D) nanosheet hybrid composite, α-Fe$_2$O$_3$ nanosheet@Ni(OH)$_2$ nanosheet, by a two-step hydrothermal method to achieve high specific capacitance and good stability performance at high charging/discharging rates when serving as electrode material of supercapacitors. The α-Fe$_2$O$_3$@Ni(OH)$_2$ hybrid electrode not only has a smooth decrease of the specific capacitance with increasing current density, compared with the sharp decline of single component of Ni(OH)$_2$ electrode, but also presents excellent rate capability with a specific capacitance of 356 F/g at a current density of 16 A/g and excellent cycling stability (a capacity retention of 93.3% after 500 cycles), which are superior to the performances of Ni(OH)$_2$ with a lower specific capacitance of 132 F/g and a lower capacity retention of 81.8% at 16 A/g. The results indicate such hybrid structure would be promising as excellent electrode material for good performances at high current densities in the future.

Energy crisis caused by the increasing consumption of fossil fuels calls for urgent development of flexible energy storage and conversion devices. Supercapacitor, also known as electrochemical capacitor (EC), with low cost, safety, long cycling life, fast charging/discharging rates and high power density, is considered to be a promising new star as energy storage devices[1,2]. They can take over batteries in electrical energy storage when meeting with short-term power boosts, such as emergency power supplies and peak power assistance in electrical equipment[3,4]. However, compared to rechargeable batteries, the critical defect of lower energy density still hinders EC's practical applications. It is highly desirable for advanced supercapacitors to have higher operating voltage, higher energy/power density and longer cycle life to meet the energy demands for practical applications in the future[5,6]. At the same time, with the increasing demand for fast charge/discharge performance of energy storage device, it is imperative for scientists to improve the performance of all aspects of supercapacitor at high current densities, including specific capacitance (C), energy density (E) and stability. Energy density can be improved by maximizing the specific capacitance and/or the cell voltage (V) according to the following equation:[5,7,8] $E = 0.5CV^2$. To increase the energy density of capacitors, pseudocapacitors, which differ from normal double-layer capacitors in energy storage, have been extensively developed to increase the operation voltage by drawing on the theory of the Faradic electrode of Li-ion batteries[9]. Therefore, pseudocapacitive materials with high specific capacitance and excellent stability at high current densities emerge as the times require.

It is generally accepted that the performance of the capacitors depends greatly on their electrode materials. Recently, abundant pseudocapacitive materials including oxides[10–12], hydroxides[13,14] and polymers[15,16] have been explored for excellent energy storage performances. Although these hydroxides or oxides have large theoretical specific capacitance and good performances in short terms, such "pseudocapacitors" often bend their knees to rate capability and reversibility during long-term Faradic redox reactions[4,17]. Nanomaterials have attracted great

[1]Department of Materials Science and Engineering, National Laboratory of Solid State Microstructures, Collaborative Innovation Center of Advanced Microstructures, Nanjing University, Nanjing 210093, P. R. China. [2]State Key Laboratory of Coordination Chemistry, Coordination Chemistry Institute, School of Chemistry and Chemical Engineering, Collaborative Innovation Center of Advanced Microstructures, Nanjing National Laboratory of Microstructures, Nanjing University, Nanjing 210093, P. R. China. [3]College of Biological and Chemical Engineering, Anhui Polytechnic University, Wuhu 241000, Anhui P. R. China. Correspondence and requests for materials should be addressed to F.G. (email: fgao@nju.edu.cn) or Q.L. (email: qylu@nju.edu.cn)
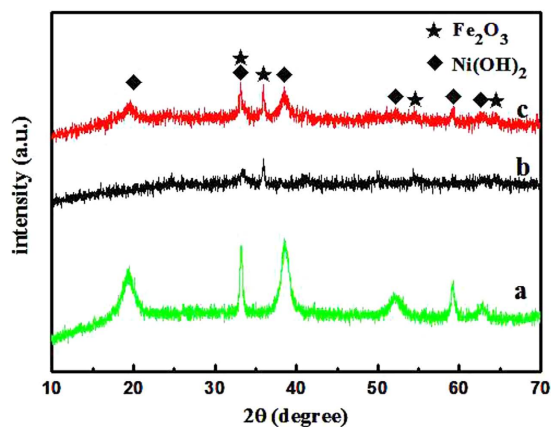
Figure 1. XRD patterns of (**a**) $Ni(OH)_2$ nanosheets; (**b**) α-Fe_2O_3 nanosheets and (**c**) α-Fe_2O_3@$Ni(OH)_2$ nanosheet hybrids.

interest in energy conversion and storage devices because of their unique electrical properties[18]. Among them, two dimensional (2D) nanomaterials, whose thickness is just several atomic layers, become the brightest stars for their high specific surface areas and abundant surface electrochemical active sites[19]. Yet, single component of 2D nanomaterials, like $Ni(OH)_2$ nanosheets, may suffer capacitance decrease after many cycles at high current densities, which prevents $Ni(OH)_2$ from being advanced electrode material. Fortunately, scientists have dedicated numerous efforts to solve the problems and achieved great successes. It is a great approach to combine two individual constituents for better electrochemical performances. For example, $Ni(OH)_2$/Graphene composite[4,5], Co_3O_4/3D Graphene[20], MnO_2@NiO[21], and 3D hybrid nanostructure $Ni(OH)_2$@Fe_2O_3[18], have significantly enhanced the capacitance and stability performance at high current densities. However, the hybrid composite consisted of two kinds of 2D inorganic graphene-like materials has not been reported.

Herein, for the first time, we presented a facile route to synthesize α-Fe_2O_3 nanosheet@$Ni(OH)_2$ nanosheet hybrid for electrode material of supercapacitor. This distinctive structure has the following advantages. Firstly, α-Fe_2O_3 and $Ni(OH)_2$ are both 2D nanosheets whose 2D structures can bring controllable electrical properties and high specific surface areas for superior electrochemical activities[19,22,23]. Secondly, the introduction of α-Fe_2O_3 can reduce the aggregation of individual $Ni(OH)_2$ nanosheets into larger assemblies[17,24,25]. Thirdly, by hybriding 2D $Ni(OH)_2$ with α-Fe_2O_3, synergetic effect is expected to give both high rate capability and good recyclability. The as-prepared α-Fe_2O_3@$Ni(OH)_2$ nanosheet hybrid exhibits excellent rate capability with a specific capacitance of 356 F/g at a current density of 16 A/g and excellent cycling stability (a capacity retention of 93.3% after 500 circles), which are superior to the performances of $Ni(OH)_2$ with a specific capacitance of 132 F/g and a capacity retention of 81.8%.

Results and Discussions

The α-Fe_2O_3 nanosheet@$Ni(OH)_2$ nanosheet hybrid was fabricated through a two-step hydrothermal route. First, ultrathin α-Fe_2O_3 nanosheets were synthesized by a metal ion intervened hydrothermal method with Al^{3+} as structure director according to our previous report[26], then $Ni(OH)_2$ nanosheets was produced onto the surface of as-prepared α-Fe_2O_3 with carboxymethylcellulose (CMC) as structure director. For comparison, the same procedure was also applied to prepare $Ni(OH)_2$ without the addition of α-Fe_2O_3. Typical X-ray diffraction (XRD) patterns of $Ni(OH)_2$, α-Fe_2O_3 and α-Fe_2O_3@$Ni(OH)_2$ hybrid are shown in Fig. 1. In Fig. 1a, all of the diffraction peaks can be indexed to hexagonal $Ni(OH)_2$ (JCPDS No. 03-0177), confirming the formation of single $Ni(OH)_2$ nanocrystals with high purity. All the diffraction peaks in Fig. 1b can be indexed to hematite α-Fe_2O_3 (JCPDS No. 33-0664) and no obvious impurity peaks can be observed, indicating the high purity of the product with the addition of Al^{3+}. After introducing $Ni(OH)_2$ onto the surface of α-Fe_2O_3, both diffraction peaks of α-Fe_2O_3 and $Ni(OH)_2$ emerge as shown in Fig. 1c, suggesting the formation of the composite composed of α-Fe_2O_3 and $Ni(OH)_2$. Figure S1 displays scanning electron microscopy (SEM) images of two single materials. As shown in Figure S1a, the obtained α-Fe_2O_3 is composed of monodisperse nanosheets with 2D size of 500 nm and thickness of about 2 nm. Figure S1b demonstrates that under the hydrothermal conditions without the addition of α-Fe_2O_3, the obtained $Ni(OH)_2$ crystals have flower-like structures assembled by nanosheets. Figure 2 shows SEM, transmission electron microscopy (TEM) and high-resolution TEM (HRTEM) images of α-Fe_2O_3@$Ni(OH)_2$ nanosheet hybrid. From the SEM images shown in Fig. 2a,b, it is clearly observed that the hybrid presents a sandwich-like structure with wrapped α-Fe_2O_3 serving as intermediate layer and attached $Ni(OH)_2$ nanosheet as coating layers. The typical structure can be clearly observed in red rectangle of Fig. 2b. The α-Fe_2O_3 nanosheets are tightly covered by $Ni(OH)_2$ nanosheets with a lot of folds. TEM images shown in Fig. 2c,d also show that the center part of the structure is much darker than the edges confirming the sandwich-like structure of the nanosheet hybrid. Central part of the image contains α-Fe_2O_3 nanosheet covered by $Ni(OH)_2$ nanosheets. Single wrinkled $Ni(OH)_2$ nanosheet occupies most parts of edge section. Further evidences can be obtained from HRTEM characterizations. Figure 2e,f show HRTEM images of different parts of the hybrids. As shown in Fig. 2e captured from central part of the TEM image, three directions of fringes with same spacings of 0.25 nm and the
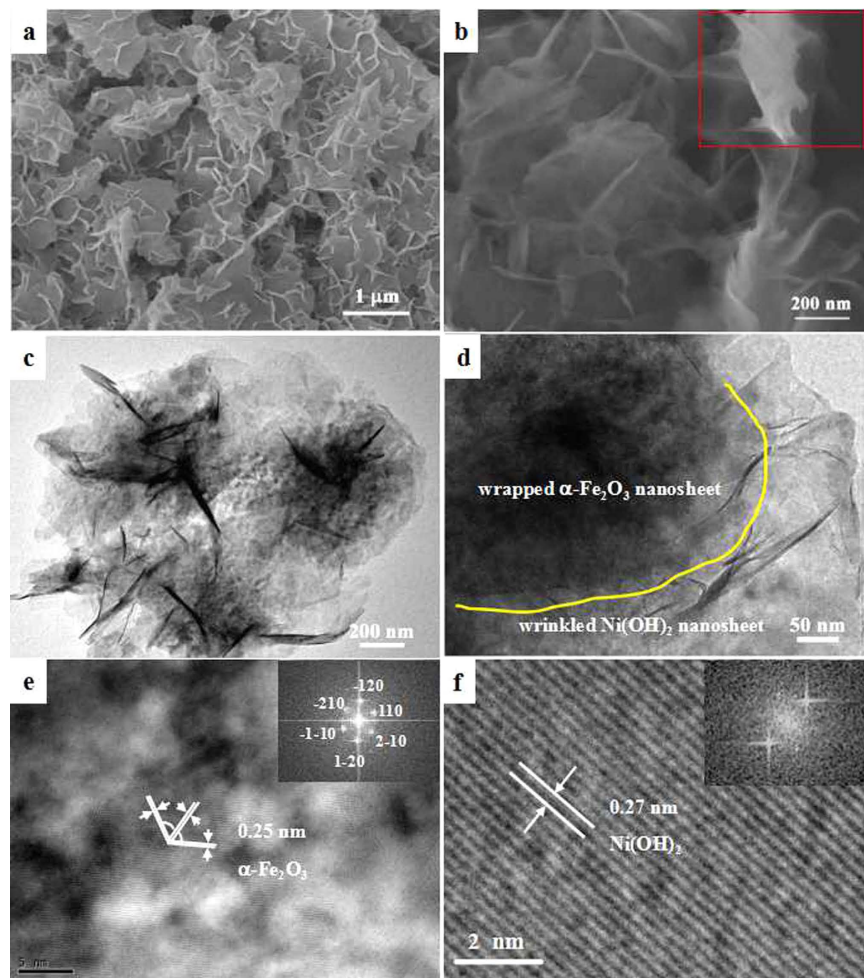
Figure 2. (**a,b**) SEM images and (**c,d**) TEM images and (e,f) HRTEM images of α-Fe$_2$O$_3$@Ni(OH)$_2$ nanosheet hybrids.

corresponding fast Fourier transform (FFT) in inset of Fig. 2e indicate that they belong to hexagonal phase of α-Fe$_2$O$_3$ (PDF: 33-0664). At the same time, HRTEM image in Fig. 2f shows perfect aligned crystal lattice planes from outer edge, corresponding to {100} planes of Ni(OH)$_2$, whose interplanar spacing is 0.27 nm. The HRTEM images presents the changes of 2D lattice fringe from inside to outside, directly proving the structure characteristic of hybrid.

Figure 3 displays the scheme of the whole synthesis process. After the formation of α-Fe$_2$O$_3$ nanosheets, they were used as templates with CMC as the directing agent. The functionalized side groups on molecular chain of CMC are easy to combine with Ni^{2+} by electrostatic force to form polymer–inorganic composite, which can work as a template to ensure the anisotropic growth of the inorganic precursor and result in the formation of inorganic nanosheets[27]. The functionalized side groups of CMC can also enable the polymer–inorganic composite to be adsorbed onto the surface of α-Fe$_2$O$_3$ nanosheets due to the interaction between the functional groups (such as carboxyl and hydroxyl groups) and Fe^{3+}. Under hydrothermal conditions, Ni(OH)$_2$ nanosheets formed coating on the surface of α-Fe$_2$O$_3$. IR spectra of α-Fe$_2$O$_3$, Ni(OH)$_2$, and Fe$_2$O$_3$@Ni(OH)$_2$ are displayed in Figure S2 with the wavenumber ranging from 4000 to 300 cm^{-1}. The sharp absorption peaks of around 3640 cm^{-1} and 533 cm^{-1} of both Ni(OH)$_2$ and α-Fe$_2$O$_3$@Ni(OH)$_2$ are related to stretching vibration and lattice vibration of hydroxyl respectively. Low wavenumber peaks around 534 cm^{-1} of α-Fe$_2$O$_3$, Ni(OH)$_2$ and α-Fe$_2$O$_3$@Ni(OH)$_2$ attribute to the lattice vibration of Ni-O, Fe-O, and nearly equal value indicates possible interaction between two compounds. Besides, the IR spectra also contain stretching (3404 cm^{-1}) and bending vibration (1610 cm^{-1}) of adsorbed water. No obvious extra peaks are observed in α-Fe$_2$O$_3$@Ni(OH)$_2$, indicating no emergence of newly functional group, which illustrates possibly simple attachment of Ni(OH)$_2$ onto the surface of α-Fe$_2$O$_3$ nanosheet.

The acquisition of the α-Fe$_2$O$_3$@Ni(OH)$_2$ hybrid gives us opportunity to investigate the electrochemical performance of such novel nanosheet composites. In general, cyclic voltammetry (CV) is used to research the capacitive behavior and reversibility of an electrode material[5]. The electrochemical tests were carried out in a three-electrode system with a Pt wire counter electrode and an Ag/AgCl reference. Figure 4a,b show the CVs of the single Ni(OH)$_2$ nanosheets and the α-Fe$_2$O$_3$@Ni(OH)$_2$ nanosheet hybrid, which were conducted at the scan rates of 5, 10, 20, 50 and 100 mV/s with potential windows ranging from 0.2 to 0.6 V. Compared to the Ni(OH)$_2$ electrode, although the CV peaks of α-Fe$_2$O$_3$@Ni(OH)$_2$ hybrid electrode broaden, the two strong redox peaks
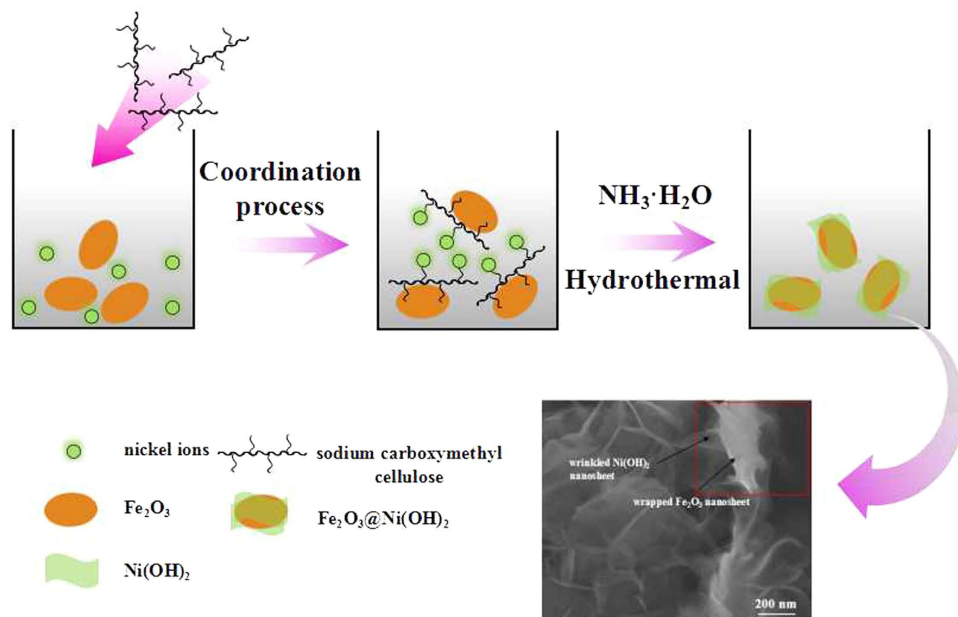
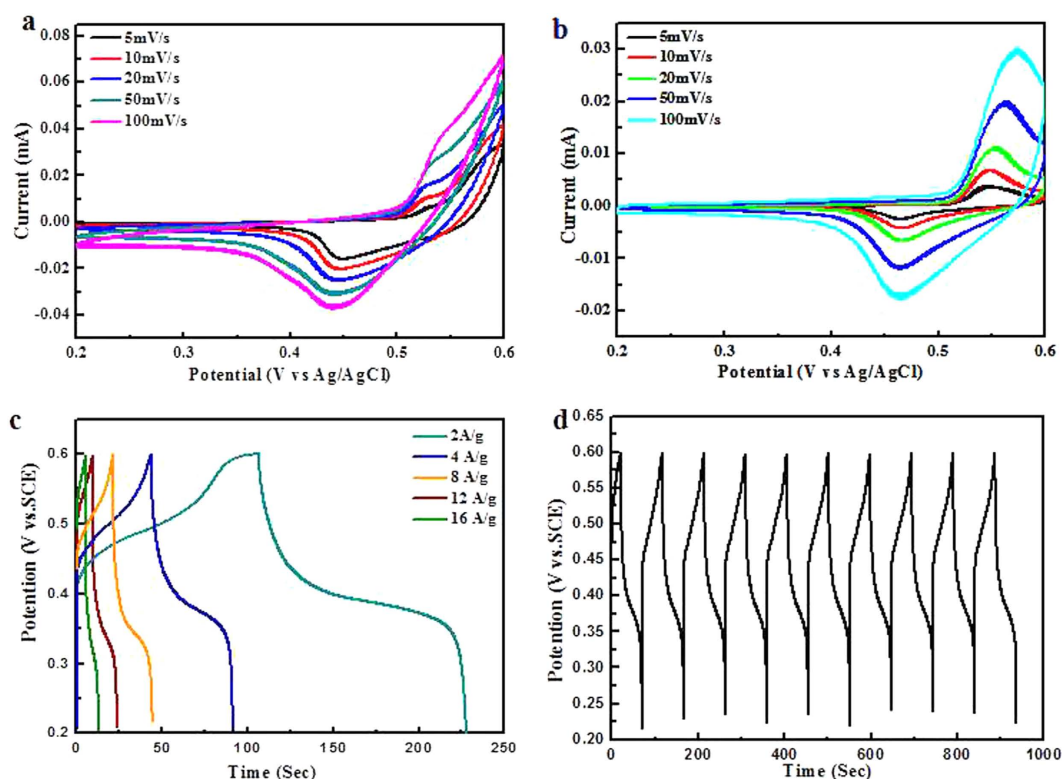**Figure 3. Schematic synthesis process of α-Fe$_2$O$_3$@Ni(OH)$_2$ nanosheet hybrid.**

Figure 4. (**a**) CV curves of Ni(OH)$_2$ nanosheets; (**b**) CV curves of α-Fe$_2$O$_3$@Ni(OH)$_2$ nanosheet hybrids; (**c**) current charge/discharge curves of hybrid electrode at different current densities and (**d**) 10 cycles of charge-discharge curves of α-Fe$_2$O$_3$@Ni(OH)$_2$ nanosheet hybrids.

still exist, which reveals the pseudocapacitance characteristics. The quasi symmetric characteristic of the redox peaks and cycles in the first few loops indicates the excellent reversibility of the Ni(OH)$_2$ and hybrid electrodes. Figure 4c shows chronopotentiometry (CP) curves of the hybrid electrode within a potential window of 0.2–0.6 V at different current densities from 2 to 16 A/g. From the CP curves, it can be observed that the discharge time is
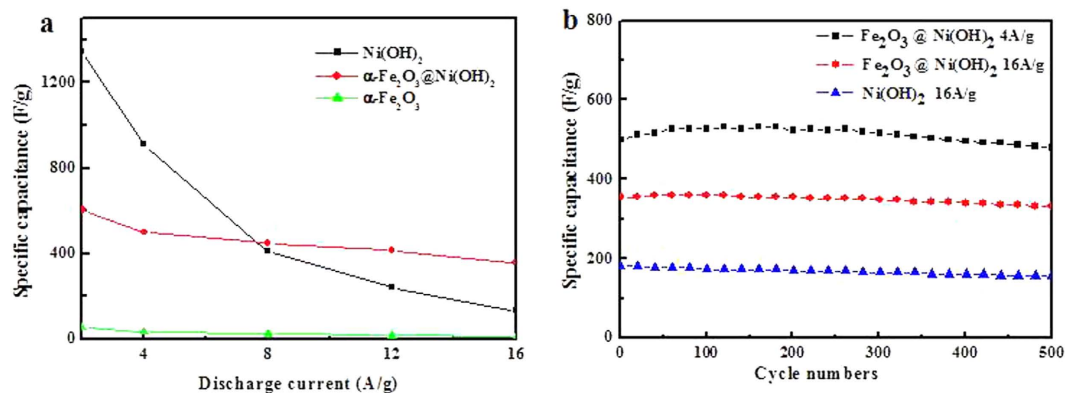
Figure 5. (**a**) Specific capacitances of α-Fe$_2$O$_3$ nanosheets, Ni(OH)$_2$ nanosheets and α-Fe$_2$O$_3$@Ni(OH)$_2$ nanosheet hybrid electrodes at different current densities; (**b**) cycling performances of the two electrodes.

longer than charge time at low current density, indicating that some undesirable reduction reaction may happen during the electrochemical process. It is also clearly observed from the CP curves that the each discharge curve contains two section: a rapid potential descent process and a slow potential decay process. The former represents a low internal resistance and the latter indicates the capacitive character of the electrode. Figure 4d shows the 10 charge-discharge cycles at a current density of 4 A/g, which indicates the superior reversible characteristics of hybrid electrode.

To study the capacitance difference of Ni(OH)$_2$ and hybrid electrodes, the CPs of Ni(OH)$_2$ and α-Fe$_2$O$_3$ nanosheets were also carried out, which are displayed in Figure S3. The specific capacitance can be calculated from CPs according to the equation: $C = (I_d \times \Delta T)/(\Delta V \times m)$, where C is the specific capacitance (F/g), I_d is discharge current(A), ΔT is discharge time (s), ΔV is the potential change (V), and m represents the mass of the active material within the electrode (g). Figure 5a shows the obvious specific capacitance difference of three electrodes at a current density of 2, 4, 8, 12 and 16 A/g, respectively, from which it can be clearly observed that α-Fe$_2$O$_3$@ Ni(OH)$_2$ hybrid electrode has a smooth decrease of specific capacitance with increasing current density, compared with the sharp decline of single component of Ni(OH)$_2$ electrode. The hybrid electrode exhibits higher specific capacitance than Ni(OH)$_2$ electrode at high current densities, despite of lower capacitance than Ni(OH)$_2$ at low current densities. As known, Ni(OH)$_2$ is a promising pseudocapacitive material due to its high specific capacity but α-Fe$_2$O$_3$ is not an ideal material for supercapacitor electrode. At low current densities, the addition of α-Fe$_2$O$_3$ would no doubt sacrifice some capacity because of the low capacitance of α-Fe$_2$O$_3$. But in the other hand the better conductivity of α-Fe$_2$O$_3$ nanosheets would make the hybrid stand up the impact of large-current, which may attribute to the enhanced conductivity to support fast electron transport required by high rates[4]. EIS tests of α-Fe$_2$O$_3$, Ni(OH)$_2$, and α-Fe$_2$O$_3$@Ni(OH)$_2$ were carried out and the curves are shown in Figure S4a. From the semicircles in the EIS curves, it can be seen that the hybridation of α-Fe$_2$O$_3$ with Ni(OH)$_2$ results in the decrease of charge-transfer resistance (Rct) comparing to that of single Ni(OH)$_2$, indicating the more facile charge transfer ability of α-Fe$_2$O$_3$@Ni(OH)$_2$ nanosheet hybrids, which may enhance the charge-discharge performance at high current densities. This is an exciting phenomenon that the rapid charging/discharging performance of Ni(OH)$_2$ can be greatly improved by combining with the ultrathin ferric oxide. It is important for supercapacitor electrodes to keep capacitance extremely with low capacitance loss at long term circulations[28]. Therefore, cycling-life tests of the hybrid and the single component of Ni(OH)$_2$ electrodes were carried out to discuss the behavior of capacitance decay. Figure 5b shows the cycling test of at a current density of 4 A/g and 16 A/g for the hybrid electrode and 16 A/g for the Ni(OH)$_2$ electrode. The hybrid electrode presents good cycle stability with a extremely high capacity retention of 96.0% at a current density of 4 A/g and 93.3% at 16 A/g after 500 cycles, confirming the good stability of hybrid electrode at both low rate and high rate. However, single component of Ni(OH)$_2$ electrode displays a poor performance with a lower capacity retention of 81.8% at a current density of 16 A/g, which illustrates again that α-Fe$_2$O$_3$@ Ni(OH)$_2$ nanosheet hybrid has an excellent performance of fast charging/discharging. At the same time, we also conducted the cycle performances of α-Fe$_2$O$_3$@Ni(OH)$_2$ and Ni(OH)$_2$ for 2000 cycles to research the long-term stability. As shown in Figure S4b after 2000 cycles, the hybrid electrode still has a higher specific capacitance than Ni(OH)$_2$ electrode with good stability. The superior electrochemical performance of hybrid electrodes can be attributed to the synergistic effects of α-Fe$_2$O$_3$ and Ni(OH)$_2$. α-Fe$_2$O$_3$ nanosheets not only provide abundant active sites for increased capacitance but also help Ni(OH)$_2$ nanosheets stabilize nanostructure at high current densities. In this case, the superiority of 2D composite materials is reflected and the hybrid has potential to be developed as an outstanding supercapacitor electrode material. It is also highly expected to explore the supercapacitor devices in the future with α-Fe$_2$O$_3$@Ni(OH)$_2$ nanosheets for high-performance supercapacitors with fast charging/discharging ability.

Conclusions

In summary, α-Fe$_2$O$_3$ nanosheet@Ni(OH)$_2$ nanosheet, a hybrid of two-dimensional ultrathin nanomaterial was synthesized and developed as electrode of supercapacitor through a simple and cost-effective approach. In such composites, α-Fe$_2$O$_3$ nanosheets serves as core and Ni(OH)$_2$ nanosheets as shell, and this distinctive design effectively shortens the ion diffusion path and provides abundant active sites, meanwhile stabilizes the structure. The

hybrid electrode presents a more smooth specific capacitance change than that of $Ni(OH)_2$ electrode with the increase of current density. The electrode based on the hybrid composites shows excellent electrochemical performances at high current densities, including the increase of specific capacitance and enhancement of stability. The specific capacitance of α-Fe_2O_3 nanosheet@$Ni(OH)_2$ nanosheet reached 356 F/g, and had a capacity retention of 93.3% at a current density of 16 A/g after 500 cycles, which was superior to the performance of $Ni(OH)_2$ with a specific capacitance of 132 F/g and a capacity retention of 81.8%. The results illustrate that the hybrid electrode has a more excellent fast charging/discharging performance at high current densities than single component of $Ni(OH)_2$. It is worthy to expect that the fabricated α-Fe_2O_3 nanosheet@$Ni(OH)_2$ nanosheet composite architectures would be applied in high-performance supercapacitors with fast charging/discharging ability and high energy/power densities in the future.

Methods

Synthesis of α-Fe_2O_3@$Ni(OH)_2$ nanosheet hybrid and $Ni(OH)_2$ nanosheets.

α-Fe_2O_3@$Ni(OH)_2$ nanosheet hybrid material was prepared via a simple two step process. First, α-Fe_2O_3 nanosheets were synthesized by applying metal ions Al^{3+} as structure-directing agents, as described in our previous work[26]. Then α-Fe_2O_3 naonosheets were added to a Teflon-lined autoclave (40 mL) containing nickel acetate and carboxymethylcellulose aqueous solution under magnetic stirring. After 30 min of stirring, appropriate amount of ammonia solution (25%, analytically pure) was added to the autoclave for further 20 min of stirring. Then the mixture was sealed, transferred to oven, and kept at 80 °C for 12 h. The red precipitate was obtained by centrifugation (10 000 rpm, 1 min) and washed with deionized water and ethanol for 3 times, and dried in air. The synthesis of $Ni(OH)_2$ nanosheet was same as α-Fe_2O_3@$Ni(OH)_2$ hybrid except the addition of α-Fe_2O_3 nanosheets.

Characterizations.

Scanning electron microscopy (SEM) was performed on Hitachi S-4800 at 10 kV. Transmission electron microscopy (TEM) and high-resolution TEM (HRTEM) images were obtained by using a JEOL JEM-2100 transmission electron microscope operating at 200 kV. Powder X-ray diffraction (XRD) patterns were collected by using a Bruker D8 ADVANCE diffractometer with CuKα radiation ($\lambda = 1.5418$ Å).

Electrochemical test.

The working electrode was obtained by mixing the electroactive material, acetylene black, and polymer binder (polyvinylidene difluoride, PVDF) in a mass ratio of 75:15:10 with solvent (N-methylpyrrolidone, NMP). Then the homogeneous slurry was coated on the pre-treated nickel foam as the working electrode after stirring for one night, and dried at 50 °C for 12 h in a vacuum oven. Finally, the Ni foam with active materials was pressed with mass loading about 1.0 mg·cm^{-2} under 10 MPa for 40 seconds. Electrochemical measurements including cyclic voltammogram (CV) and chronopotentiometry (CP) were operated using a three-electrode system with a CHI 660 d electrochemical workstation in an electrolyte aqueous KOH electrolyte (1.0 M). A Pt wire was used as the counter electrode and a Ag/AgCl electrode was served as the reference electrode. In details, CV experiments were performed at various scan rates of 5, 10, 20, 50, and 100 mV/s. CP charge/discharge curves were obtained at various current densities of 2, 4, 8, 12 and 16 A/g to evaluate the specific capacitance. A potential window in the range from 0.2 to 0.6 V was used during all measurements.

References

1. Ji, J. Y. *et al.* Nanoporous $Ni(OH)_2$ Thin Film on 3D Ultrathin-Graphite Foam for Asymmetric Supercapacitor. *ACS Nano* **7,** 6237–6243 (2013).
2. Wang, G. P., Zhang, L. & Zhang, J. J. A Review of Electrode Materials for Electrochemical Supercapacitors. *Chem. Soc. Rev.* **41,** 797–828 (2012).
3. Simon, P. & Gogotsi, Y. Materials for Electrochemical Capacitors. *Nat. Mater.* **7,** 845–854 (2008).
4. Wang, H. L., Casalongue, H. S., Liang, Y. Y. & Dai, H. J. $Ni(OH)_2$ Nanoplates Grown on Graphene as Advanced Electrochemical Pseudocapacitor Materials. *J. Am. Chem. Soc.* **132,** 7472–7477 (2010).
5. Yan, J. *et al.* Advanced Asymmetric Supercapacitors Based on $Ni(OH)_2$/Graphene and Porous Graphene Electrodes with High Energy Density. *Adv. Funct. Mater.* **22,** 2632–2641 (2012).
6. Izadi-Najafabadi, A. *et al.* Extracting the Full Potential of Single-Walled Carbon Nanotubes as Durable Supercapacitor Electrodes Operable at 4 V with High Power and Energy Density. *Adv. Mater.* **22,** E235–E241 (2010).
7. Demarconnay, L., Raymundo-Pinero, E. & Béguin, F. Adjustment of Electrodes Potential Window in an Asymmetric Carbon/MnO_2 Supercapacitor. *J. Power Sources* **196,** 580–586 (2011).
8. Chen, P. C., Shen, G. Z., Shi, Y., Chen, H. T. & Zhou, C. W. Preparation and Characterization of Flexible Asymmetric Supercapacitors Based on Transition-Metal-Oxide Nanowire/Single-Walled Carbon Nanotube Hybrid Thin-Film Electrodes. *ACS Nano* **4,** 4403–4411 (2010).
9. Wu, Z. S. *et al.* High-Energy MnO_2 Nanowire/Graphene and Graphene Asymmetric Electrochemical Capacitors. *ACS Nano* **4,** 5835–5842 (2010).
10. Zhang, H. *et al.* Growth of Manganese Oxide Nanoflowers on Vertically-Aligned Carbon Nanotube Arrays for High-Rate Electrochemical Capacitive Energy Storage. *Nano Lett.* **8,** 2664–2668 (2008).
11. Wei, W. F., Cui, X. W., Chen, W. X. & Ivey, D. G. Manganese Oxide-based Materials as Electrochemical Supercapacitor Electrodes. *Chem. Soc. Rev.* **40,** 1697–1721 (2011).
12. Rakhi, R. B., Chen, W., Hedhili, M. N., Cha, D. K. & Alshareef, H. N. Enhanced Rate Performance of Mesoporous Co_3O_4 Nanosheet Supercapacitor Electrodes by Hydrous RuO_2 Nanoparticle Decoration. *ACS Appl. Mater. Interfaces.* **6,** 4196–4206 (2014).
13. Chou, S. L., Wang, J. Z., Liu, H. K. & Dou, S. X. Electrochemical Deposition of Porous $Co(OH)_2$ Nanoflake Films on Stainless Steel Mesh for Flexible Supercapacitors. *J. Electron. Mater.* **155,** A926–A929 (2008).
14. Yang, G. W., Xu, C. L. & Li, H. L. Electrodeposited Nickel Hydroxide on Nickel Foam with Ultrahigh Capacitance. *Chem. Commun.* 6537–6539 (2008).
15. Meng, C. Z., Liu, C. H., Chen, L. Z., Hu, C. H. & Fan, S. S. Highly Flexible and All-Solid-State Paperlike Polymer Supercapacitors. *Nano Lett.* **10,** 4025–4031 (2010).
16. Roberts, M. E., Wheeler, D. R., McKenzie, B. B. & Bunker, B. C. High Specific Capacitance Conducting Polymer Supercapacitor Electrodes Based on Poly(tris(thiophenylphenyl)amine). *J. Mater. Chem.* **19,** 6977–6979 (2009).

17. Tian, W. *et al.* Ni(OH)$_2$ Nanosheet@Fe$_2$O$_3$ Nanowire Hybrid Composite Arrays for High-Performance Supercapacitor Electrodes. *Nano Energy* **2,** 754–763 (2013).
18. Arico, A. S., Bruce, P., Scrosati, B., Tarascon, J. M. & Schalkwijk, W. V. Nanostructured Materials for Advanced Energy Conversion and Storage Devices. *Nat. Mater.* **4,** 366–377 (2005).
19. Peng, X., Peng, L. L., Wu, C. Z. & Xie, Y. Two Dimensional Nanomaterials for Flexible Supercapacitors. *Chem. Soc. Rev.* **43,** 3303–3323 (2014).
20. Dong, X. C. *et al.* 3D Graphene Cobalt Oxide Electrode for High-Performance Supercapacitor and Enzymeless Glucose Detection. *ACS Nano* **6,** 3206–3213 (2012).
21. Liu, J. P., Jiang, J., Bosmanc, M. & Fan, H. J. Three-Dimensional Tubular Arrays of MnO$_2$-NiO Nanoflakes with High Areal Pseudocapacitance. *J. Mater. Chem.* **22,** 2419–2426 (2012).
22. Compton, O. C. & Nguyen, S. B. T. Graphene Oxide, Highly Reduced Graphene Oxide, and Graphene: Versatile Building Blocks for Carbon-Based Materials. *Small* **6,** 711–723 (2010).
23. Xiong, F., Liao, A. D., Estrada, D. & Pop, E. Low-Power Switching of Phase-Change Materials with Carbon Nanotube Electrodes. *Science* **232,** 568–570 (2011).
24. Wang, Y. L. *et al.* Hierarchical SnO$_2$-Fe$_2$O$_3$ Heterostructures as Lithium-Ion Battery Anodes. *J. Mater. Chem.* **22,** 21923–21927 (2012).
25. Wang, G. *et al.* Synthesis and Evaluation of Carbon-Coated Fe$_2$O$_3$ Loaded on Graphene Nanosheets as an Anode Material for High Performance Lithium Ion Batteries. *J. Power Sources.* **239,** 37–44 (2013).
26. Liu, R. M., Jiang, Y. W., Lu, Q. Y., Du, W. & Gao, F. Al^{3+}-Controlled Synthesis and Magnetic Property of α-Fe$_2$O$_3$ Nanoplates. *CrystEngComm* **15,** 443–446 (2013).
27. Wang, L. F. *et al.* Generalized Low-Temperature Fabrication of Scalable Multi-Type Two-Dimensional Nanosheets with a Green Soft Template. *Chem. Eur. J.* **22,** 5575–5582 (2016).
28. Hou, Y., Cheng, Y. W., Hobson, T. & Liu, J. Design and Synthesis of Hierarchical MnO$_2$ Nanospheres/Carbon Nanotubes/Conducting Polymer Ternary Composite for High Performance Electrochemical Electrodes. *Nano Lett.* **10,** 2727–2733 (2010).

Acknowledgements

Author Contributions

Q.L. and F.G. guided the entire project, carried out data analyses and co-wrote the manuscript. H.J., H.M. and Y.J. performed the experiments, XRD characterizations, and SEM investigations. L.W. performed TEM investigations. All the coauthors discussed the results and commented on the manuscript.

Additional Information

Supplementary information accompanies this paper at http://www.nature.com/srep

Competing financial interests: The authors declare no competing financial interests.

How to cite this article: Jiang, H. *et al.* Hybrid α-Fe$_2$O$_3$@Ni(OH)$_2$ nanosheet composite for high-rate-performance supercapacitor electrode. *Sci. Rep.* **6**, 31751; doi: 10.1038/srep31751 (2016).